remote sensing

MDPI

Article

GIS-Based Assessment of Shaded Road Segments for Enhanced Winter Risk Management

Miguel Ángel Maté-González *, Cristina Sáez Blázquez, Daniel Herranz Herranz, Sergio Alejandro Camargo Vargas and Ignacio Martín Nieto

Department of Cartographic and Land Engineering, Higher Polytechnic School of Avila, University of Salamanca, Hornos Caleros 50, 05003 Avila, Spain; u107596@usal.es (C.S.B.); danielherranz@usal.es (D.H.H.); sacamargov@usal.es (S.A.C.V.); nachomartin@usal.es (I.M.N.)
* Correspondence: mategonzalez@usal.es

Highlights

What are the main findings?

- Persistent topographic shading is identified as a primary driver of frost and ice persistence on mountainous road pavements, independent of regional climatic conditions.
- High-resolution solar incidence modelling, validated with UAV-based thermal orthophotos, reliably detects micro-scale cold-prone road segments.

What are the implications of the main findings?

- Shadow persistence mapping enables proactive winter maintenance planning, allowing targeted de-icing, signage placement, and resource optimization.
- The methodology provides a decision-support framework for selecting priority road segments for climate-resilient interventions, including geothermal road-heating systems.

Abstract

Winter road safety is critically influenced by microclimatic factors that determine where frost and ice persist on pavement surfaces. Among these, shadow duration plays a decisive yet often under quantified role in mountainous regions, where complex topography and variable solar exposure create localized cold zones. This study presents a GIS-based methodology for detecting and characterizing shadow-prone areas along high-altitude roads, extending previous national-scale models of winter risk toward local, geometry-driven analysis. Using high-resolution Digital Terrain Models (DTM02) and solar radiation simulations, four representative mountain roads (CL-505, AV-501, and CA-820) were analyzed to evaluate how orientation, slope, and surrounding relief control solar incidence. The resulting shadow maps were validated through UAV-derived thermal orthophotos and ground-based temperature measurements, confirming strong correspondence between simulated low-irradiance areas and observed cold surfaces. The integration of geometric and radiometric data demonstrates that topographic shading is a reliable predictor of frost persistence and can be incorporated into winter maintenance planning. By combining high-resolution terrain analysis with empirical thermal validation, this approach not only enhances predictive accuracy but also provides actionable insights for prioritizing road sections at greatest risk. Ultimately, it offers a scalable, data-driven framework for improving infrastructure resilience, optimizing maintenance operations, and mitigating winter hazards in cold-climate mountainous environments, supporting both safety and cost-effectiveness in road management strategies.

Academic Editor: Wen Liu

Received: 14 December 2025
Revised: 27 January 2026
Accepted: 28 January 2026
Published: 2 February 2026

Keywords: road icing; geospatial analysis; solar incidence; thermal remote sensing; UAV thermography; winter risk mapping; road safety; infrastructure management

1. Introduction

Winter road safety continues to be one of the most pressing challenges in the management of modern transportation infrastructure, as icy and snow-covered roads can lead to increased accident rates, traffic disruptions, and significant economic losses [1,2]. Adverse winter conditions not only compromise the mobility of commuters and freight transport but also strain maintenance resources, requiring timely interventions such as de-icing, snow removal, and monitoring of hazardous road sections. Moreover, the complex interplay of meteorological, topographical, and infrastructural factors makes predicting and mitigating winter hazards particularly challenging, highlighting the need for advanced, spatially explicit modelling approaches and targeted risk management strategies [3,4]. In this sense, the simultaneous occurrence of icing, reduced pavement temperatures, and limited driver visibility is particularly pronounced in shadowed areas, where the absence of solar radiation prevents surfaces from warming during daylight hours. These shaded road sections often retain frost and ice long after adjacent, sun-exposed areas have thawed, thereby increasing the likelihood of accidents and necessitating disproportionately high maintenance interventions. In mountainous regions, where complex topography amplifies microclimatic variability, shading emerges as a critical factor influencing pavement surface conditions. Despite its significance, shading remains one of the least quantified parameters in conventional road infrastructure assessments, limiting the ability to implement targeted risk mitigation strategies. Understanding the spatial and temporal dynamics of shaded areas is therefore essential to enhance winter road safety and optimize maintenance resource allocation [5–8].

Across Europe, the social and economic impacts of adverse winter conditions are substantial. Studies indicate that frost- and ice-related accidents represent a significant percentage of road incidents during cold months, while maintenance operations to mitigate these risks consume large portions of public budgets [9]. In Spain, for example, the annual cost of snow and ice control in the national network has steadily increased due to the climatic variability and the rising frequency of extreme meteorological events [10]. Beyond direct economic losses, such conditions compromise mobility, disrupt logistics, and increase greenhouse gas emissions due to congestion and detours [11,12]. The combined effects of accidents, mobility restrictions, and environmental impacts illustrate the multifaceted nature of winter hazards, emphasizing the need for advanced risk assessment strategies. These challenges highlight the critical importance of accurate, spatially explicit tools capable of predicting and mitigating winter hazards.

In this context, previous research has demonstrated that elements such as low temperatures, elevation, and precipitation are the main drivers of winter road hazards across large territories [13,14]. Additionally, different national-scale models integrating factors such as altitude, climatic zones, average winter precipitation, and satellite-derived surface temperatures have been widely used to identify areas most exposed to frost and ice formation. These models provide a predictive framework for winter risk management by combining topographic, climatic, and remote sensing datasets through multivariate Geographical Information System (GIS) analysis, including normalization, raster algebra, and correlation matrices, to generate continuous winter risk indices. Such approaches effectively delineate cold-exposed regions and can be validated against operational winter maintenance plans and infrastructure data, such as the distribution of salt storage facilities and other relevant actions [15–17].

However, while these models provide a robust national-scale perspective, they also reveal a key limitation: the persistence of frost at a local scale is not solely dependent on temperature and elevation but is strongly influenced by solar exposure. Even within the same climatic zone, variations in slope orientation, road alignment, terrain configuration, and nearby obstacles (such as cut slopes, embankments, or tree cover) create microenvironments where shading significantly alters the surface energy balance [18]. These localized effects can determine whether a road segment remains icy for hours after adjacent areas have thawed. Nevertheless, few large-scale studies explicitly address the spatial and temporal behavior of shadows on road infrastructure, despite their critical influence on winter hazard formation and persistence [19,20].

Recent advances in solar radiation modelling and high-resolution terrain data have made it possible to simulate shading conditions with unprecedented precision. Using Digital Terrain Models (DTM), solar geometry equations, and radiative transfer algorithms, it is possible to estimate the duration and intensity of sunlight received by each point on the surface for specific dates and times [21]. In parallel, the development of Unmanned Aerial Vehicle (UAV)-based thermal photogrammetry has provided a valuable means to validate these simulations empirically [22,23]. Thermal orthophotos obtained from drones equipped with infrared sensors capture surface temperature patterns that directly reflect shadow persistence and the differential heating of pavements, allowing quantitative comparison with modelled shading maps [24]. This synergy between modelling and direct observation enables a more complete understanding of how topography and solar incidence influence winter risk at the micro-scale.

Building on the discussion above, the present research addresses the mentioned gap by focusing exclusively on the identification and characterization of shadow-prone areas, and by validating the results through a multi-scale observational strategy. This approach combines UAV-based thermal orthophotos with ground-based temperature measurements and terrestrial thermal imaging. The objective is not to estimate absolute heat fluxes but to detect, classify, and compare zones of persistent shade that favor ice retention under winter conditions. Using high-resolution Digital Terrain Models (DTM25) provided by the Spanish National Geographic Institute (IGN), solar radiation simulations were performed to map hourly and seasonal shadow patterns. The methodological framework is based on a national-scale winter risk modelling approach, extending it to a local, microclimatic perspective where empirical validation using UAV and in situ thermal measurements ensures the robustness of the results.

The remainder of this paper is organized as follows. Section 2 describes the datasets and methodological workflow used to detect and quantify shaded areas, detailing the solar radiation modelling process, the configuration of UAV flights, and the procedures for ground-based thermal and temperature validation. Section 3 presents the results obtained for the four selected mountain road segments, highlighting the spatial distribution of shadows and their correspondence with the thermal observations. Section 4 discusses the implications of these findings for winter road management and infrastructure planning in mountainous environments. Finally, Section 5 summarizes the main conclusions and outlines future research directions aimed at integrating shadow persistence analysis into broader geospatial risk assessment frameworks.

2. Materials and Methods

2.1. Baseline Datasets and Previous Winter Risk Layers

As mentioned above, this research builds upon previous developments by the authors, which establish a national-scale geospatial framework to evaluate the vulnerability of road infrastructure to winter conditions across mainland Spain. That earlier study integrated multi-source climatic and topographic information into a Winter Risk Index (R_x) designed to quantify the relative exposure of each area to frost and ice formation.

The model was constructed using four key environmental variables that jointly describe the spatial distribution of cold risk factors:

- Altitude (m): obtained from the Digital Terrain Model at 25 m resolution (DTM25), provided by the Spanish National Geographic Institute (IGN). Elevation plays a fundamental role in determining local temperature gradients, atmospheric pressure, and precipitation phase (rain vs. snow). Vegetation height was additionally represented using the official Vegetation Digital Surface Model provided by the IGN, the MDSnV v2.5 dataset (also referred to as NDSM–VEGETATION), in order to include canopy-induced shading effects in forested road segments.
- Climatic zonation: derived from the national climatic atlas and regional classification schemes, identifying distinct thermal regimes based on long-term averages of temperature and continentality. This variable captures the macroclimatic context and defines the general spatial limits of cold-prone regions.
- Mean January precipitation (mm/h): calculated from GPM IMERG V6 satellite data (2013–2023). Precipitation during the coldest month was selected as a proxy for the frequency of potential snow or freezing rain events, directly influencing the likelihood of ice formation on roads.
- Minimum land surface temperature (°C): extracted from satellite thermal datasets, filtered to emphasize areas that regularly drop below the critical freezing threshold. This layer provided spatially continuous thermal information, complementing point-based meteorological data.

Each variable was normalized to a common scale between 0 and 1, ensuring comparability across datasets with different physical units. The variables were then combined using a weighted additive model [25], where altitude (N_H) and temperature (N_T) were given dominant influence, while precipitation (N_R) was introduced with a smaller weight (0.1), as expressed by the following Equation (1):

$$R_W = N_H + N_T + (0.1 \cdot N_R) \tag{1}$$

The resulting Winter Risk Index (R_W) provided a synthetic representation of the country's relative susceptibility to winter-related hazards. Figure 1 illustrates the main input layers: altitude (a), temperature (b), and precipitation (c) and the final composite maps (d,e). Red and orange tones indicate areas of high winter hazard, corresponding primarily to mountain systems such as the Cantabrian Range, the Iberian System, and the Pyrenees, as well as certain elevated plateaus of the Central System.

Validation of that national-scale model demonstrated a proper agreement with official winter maintenance networks, salt storage locations, and known zones of frequent frost, confirming its utility as a predictive tool for strategic planning. However, the index was conceived for regional to national analysis, with a spatial resolution sufficient to identify cold regions but not to describe the microclimatic variability occurring at the road scale.

$$R_W = N_H + N_T + (0.1 \cdot N_R)$$

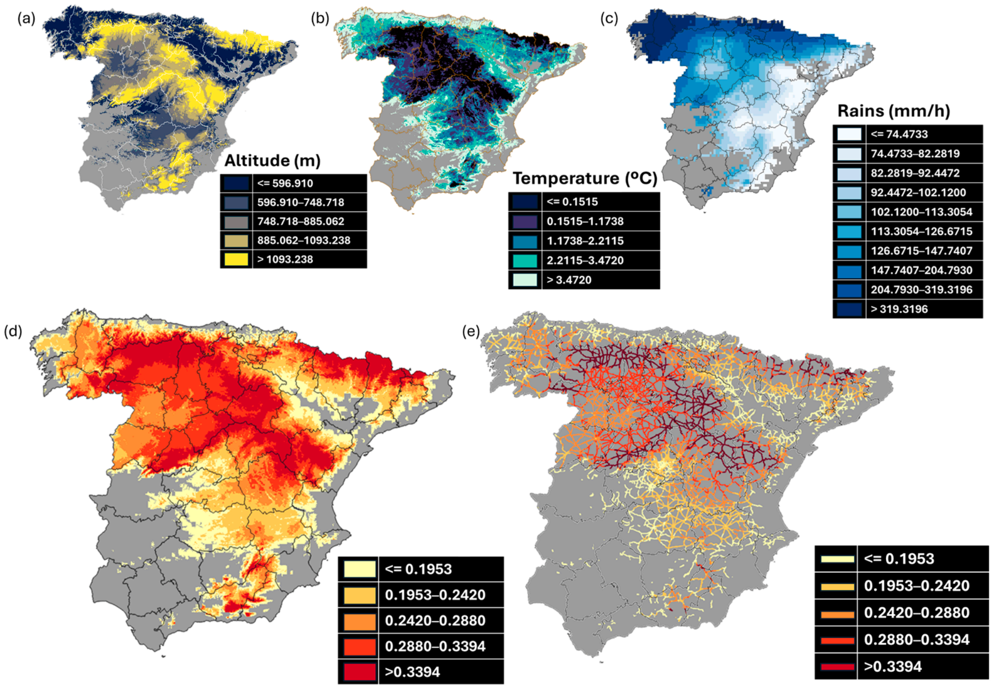

Figure 1. (**a**) Altitude; (**b**) Filtered minimum temperature; (**c**) Mean January precipitation (GPM IMERG V6); (**d**) Composite winter risk index; (**e**) Index applied to the national road network. Normalized values 0–1 indicate relative severity.

In the present study, the outputs of that framework are not recalculated but are instead used as reference layers. They serve to contextualize the selection of four representative case studies located in areas of high winter risk, as identified by the previous model. Each case corresponds to a mountain road segment characterized by steep terrain, strong orientation gradients, and limited solar exposure, conditions under which the persistence of shade is expected to enhance ice formation and delay surface thawing.

The choice of these locations allows for a focused local-scale analysis where spatial resolution and topographic complexity require more detailed modelling. By moving from a nationwide, statistically driven approach to a site-specific, physically based model, the present research aims to isolate the effect of terrain shading as a critical factor in winter road hazard dynamics. Unlike the previous framework, which estimated thermal vulnerability indirectly through temperature proxies, this work explicitly quantifies shadow duration and persistence, providing a geometrically derived indicator that complements the earlier thermal-based risk assessment.

In summary, based on the previous developments (identifying where cold-prone areas are most likely to occur), the current research investigates why and how certain locations within those areas experience prolonged icing conditions due to solar obstruction. This methodological continuity ensures methodological coherence, linking large-scale risk mapping with detailed local diagnostics applicable to winter maintenance planning and road safety management.

2.2. Shadow Mapping Methodology

For the validation phase of the proposed methodology, a mountain road section particularly affected by severe winter conditions were selected as a representative case study. This area exhibits frequent frost and ice accumulation, providing an ideal environment to test the accuracy and operational relevance of solar incidence and shading models under real conditions. The objective is to verify the correlation between theoretical solar exposure (derived from geometric and radiative models) and empirical surface temperature data collected in the field.

The study begins with a geometric segmentation of the road into homogeneous subsections based on design and morphometric parameters. This segmentation is performed in 2 m sections, corresponding to the spatial resolution of the DTM02 used, which allows for capturing geometric and morphometric variations accurately without additional interpolation. For each segment, three primary geometric descriptors are calculated: orientation (aspect), slope, and superelevation (cant). These parameters define how each portion of the pavement interacts with incoming solar radiation, determining its energy balance and potential for frost persistence.

Subsequently, for every road segment, solar incidence angles can be computed at hourly intervals throughout the day and for representative periods of the year (for each study case angles have been calculated depending on the flight period and time). This temporal simulation provides an estimate of the effective energy exposure of the surface and helps identify zones that receive limited sunlight. The methodology allows capturing shorter-term transitions, such as brief shadow-edge effects, provided that the solar position, the orientation of each analyzed point, and the instantaneous shadow pattern are simulated for each time step. The precision of the irradiance assessment can be increased as desired, as long as the corresponding parameters are explicitly included in the calculation for every simulation step.

To ensure radiative accuracy, atmospheric attenuation is also integrated into the model through the Kasten and Young [26] formulation, which corrects irradiance according to solar elevation and atmospheric path length. This correction is especially relevant under winter conditions, when the solar altitude remains low for most of the day, amplifying the influence of aerosols, humidity, and air density on radiation transmission. The analytical results are later contrasted with empirical data acquired through thermal technologies: UAV-based infrared imagery, terrestrial thermal cameras, and in situ contact thermometers embedded in the asphalt. These datasets provide independent observations that serve as ground truth, enabling quantitative assessment of model reliability [27,28].

Finally, a series of thematic maps are generated showing the effective irradiance and relative solar exposure of each road segment. These maps highlight critical cold spots where the geometric configuration and atmospheric conditions combine to reduce solar input, thereby increasing frost risk. The identification of such sections supports maintenance planning, resource allocation, and preventive safety measures. The following Figure 2 illustrates the general workflow summarizing the main steps of the proposed methodology.

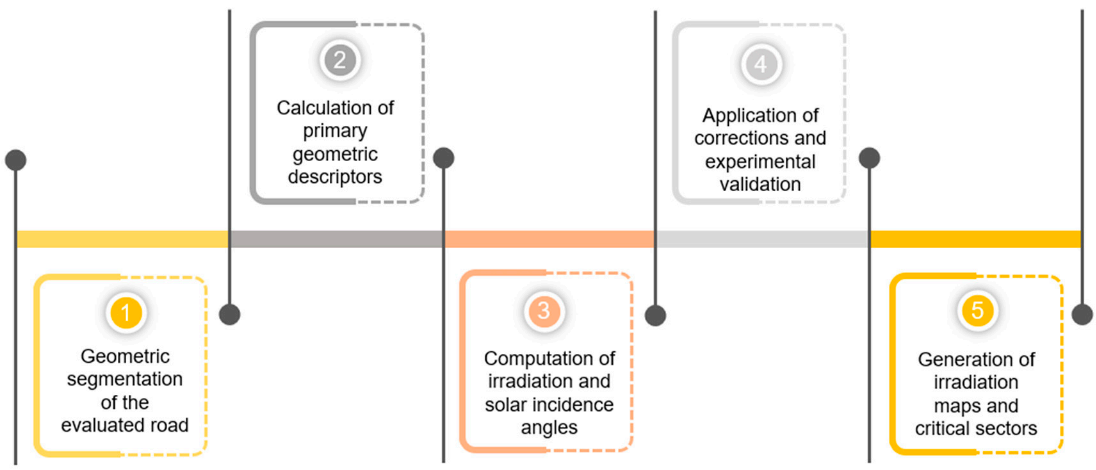

Figure 2. Workflow diagram of the road irradiance analysis methodology.

2.2.1. Solar Incidence and Irradiance Models

The estimation of solar incidence is fundamental for understanding the thermal dynamics of pavement surfaces. Solar energy input governs the rate at which surfaces heat and cool, directly influencing the persistence of frost and the probability of ice formation. Road sections that remain shaded or exposed to low incidence angles tend to exhibit lower surface temperatures, sustaining hazardous conditions for longer durations.

Geometric basis of solar incidence

The geometric framework of the road surface determines how sunlight reaches it. Each segment is defined by its slope (β), orientation or aspect (γ) and superelevation, which modify the local inclination relative to the horizontal plane. In the northern hemisphere, south-facing slopes receive greater irradiance, while north-facing slopes are often shaded, particularly during winter months.

These geometric attributes are combined with the solar elevation angle (α) (the height of the sun above the horizon) and the solar azimuth (ϕ) (its direction relative to true north) to compute the angle of solar incidence (θ) for any moment of the day or year (Equation (2)) [29]:

$$\theta = cos^{-1}(sin\alpha \cdot cos\beta + cos\alpha \cdot sin\beta \cdot cos(\phi - \gamma)) \quad (2)$$

Values of θ close to 0° indicate perpendicular radiation and maximum energy input, whereas those approaching 90° correspond to grazing incidence and minimal heating. By applying this formulation over time, a continuous map of effective solar exposure can be derived, revealing areas that remain under low-angle illumination or complete shadow.

Atmospheric attenuation and air mass correction

While the geometric model defines potential exposure, it does not account for atmospheric attenuation, the process by which solar radiation is scattered and absorbed before reaching the surface. Scattering is primarily caused by air molecules and aerosols, whereas absorption results from gases such as ozone, water vapor, and carbon dioxide. These effects intensify when the solar elevation is low, precisely the condition that characterizes high-latitude winters and mountainous terrain.

To incorporate this attenuation, the air mass factor (m) is used, representing the relative path length of sunlight through the atmosphere compared with its minimum at zenith. The empirical model proposed by Kasten and Young [26] provides a widely validated expression for this factor (Equation (3)):

$$m = \frac{1}{cos\alpha + 0.50572 \cdot (96.07995 - \alpha)^{-1.6364}} \quad (3)$$

In the previous Equation (3), α is expressed in degrees. As α increases (sun higher in the sky), m approaches 1, indicating minimal atmospheric thickness. Conversely, when α decreases near sunrise or sunset, m increases rapidly, signifying a longer optical path and greater attenuation of solar irradiance.

The original Kasten and Young [26] equation assumes a reference where 0° corresponds to zenith and 90° to the horizon. In this study, the convention is inverted, with 0° corresponding to the horizon and 90° to the zenith. To maintain consistency, the expression is reformulated as follows (Equation (4)):

$$m = \frac{1}{sin\alpha + 0.50572 \cdot (\alpha + 6.07995)^{-1.6364}} \quad (4)$$

The above adjustment ensures mathematical equivalence with the original formulation and compatibility with the elevation convention used in the model.

Corrected solar irradiance

Once the air mass factor is known, the effective irradiance (I) reaching the surface can be estimated according to (Equation (5)) [30]:

$$I = I_0 \cdot e^{-k \cdot m} \quad (5)$$

where:

I_0 = is the extraterrestrial solar irradiance (≈1367 W/m^2).

k = is the atmospheric attenuation coefficient, depending on aerosol content and humidity. A standard value of 0.14 is used under static reference conditions to estimate the fraction of energy received, without considering dynamic atmospheric variations.

m = is the air mass, as computed above.

Because this study focuses on relative spatial variability rather than absolute energy flux, irradiance values are normalized so that I_0 = 1. The resulting dimensionless parameter expresses relative transmissivity between 0 (maximum attenuation) and 1 (no attenuation), providing a consistent scale for integration with other normalized geospatial variables.

Practical implications for road analysis

The combination of the geometric incidence (θ) and the atmospheric correction (I) allows the creation of spatiotemporal irradiance maps representing the effective solar input for each road segment. These maps identify sections with consistently low energy receipt, which correspond to areas most prone to frost persistence.

The practical implications that this analysis involves are considerable:

- Safety prioritization: highlighting critical segments supports targeted deployment of de-icing materials, signage, and monitoring systems.
- Temporal analysis: evaluating solar input across seasons reveals when and where shadow effects are most significant.
- Design and maintenance optimization: understanding illumination patterns aids decisions on road alignment, vegetation management, and material selection to mitigate long-term risks.

Vegetation effects were incorporated into the shading simulations using official vegetation height information provided by the IGN. Specifically, we employed the Vegetation Digital Surface Model MDSnV v2.5 (2nd coverage), also referred to as NDSM–VEGETATION. This product is a LiDAR derived normalized digital surface model representing vegetation height above ground level.

To account for canopy obstruction, the vegetation height raster was combined with the 2 m Digital Terrain Model (DTM02) through raster algebra in QGIS v3.4, generating an enhanced elevation surface that integrates both terrain morphology and above-ground vegetation structures. This vegetation-adjusted surface was subsequently used as input for solar radiation and shadow simulations performed with the GRASS GIS (Geographic Resources Analysis Support System) toolset, an open-source geospatial analysis framework widely used for terrain-based environmental modelling. In particular, the modules r.sunmask and r.sun.insoltime were applied to model shadow persistence and solar exposure more realistically in forested road corridors.

By integrating the geometric and radiative modelling of solar incidence with complementary climatic and precipitation data and validating the outcomes through UAV and ground-based thermal observations, the proposed framework establishes a comprehensive strategy for identifying road sections most exposed to persistent frost. Its modular design enables straightforward adaptation to diverse geographical contexts and climatic regimes. Furthermore, the methodology can be extended to assess the potential evolution of winter hazards under projected climate change scenarios, thereby offering a practical and scalable tool for enhancing the long-term resilience and safety of transportation infrastructure.

2.2.2. UAV-Based Thermal Surveys and Photogrammetric Processing

To empirically validate the proposed model, an aerial campaign was conducted using a DJI Matrice 350 RTK UAV (DJI company, Shenzhen, China) equipped with a Zenmuse H20T multisensor payload (DJI company, Shenzhen, China), combining high-resolution RGB and radiometric thermal imaging. The flight plan consisted of parallel paths with approximately 80% forward and 70% side overlap, at altitudes of 100 m AGL, providing ground resolutions between 10–20 cm/pixel. The onboard RTK system ensured centimetre-level georeferencing accuracy [31,32].

Thermal and RGB datasets were processed using GRAPHOS v2.0.0.beta.8 (inteGRAted PHOtogrammetric Suite), following a standardized photogrammetric pipeline [33]:

1. Radiometric pre-processing of thermal images and synchronization with RGB frames.
2. Automatic feature extraction and tie point matching across both datasets.
3. Bundle adjustment integrating RTK metadata to refine orientation and camera parameters.
4. Dense point cloud generation through multi-view stereo reconstruction.
5. Ortho-mosaicking and thermal calibration, producing georeferenced thermal orthophotos.

These orthophotos provide a spatially continuous depiction of surface temperature variations, allowing direct comparison between predicted low-irradiance zones and observed cold surfaces. The correlation between modelled shading and thermal anomalies serves as a validation metric for the methodology.

2.2.3. Ground-Based Thermal and Temperature Measurements

Complementing the aerial surveys, ground-based thermal and temperature observations were performed to obtain high-accuracy reference data. A FLIR T540 handheld thermal camera (Teledyne FLIR LLC, Wilsonville, OR, USA) (infrared resolution 464 $\times$ 348 px, thermal sensitivity < 0.04 °C at 30 °C, and absolute accuracy $\pm$ 2 °C or $\pm$2% of reading) was used to capture detailed surface temperature distributions at selected points along the road, particularly during dawn and dusk, when contrasts between shaded and sunlit areas are most pronounced. These thermal images allow the identification of localized cold spots such as shaded gullies, forested edges, and cut slopes that tend to accumulate frost.

In parallel, Testo 110 probe-type contact thermometers (measurement range -50 °C to +400 °C, accuracy $\pm$ 0.3 °C, resolution 0.1 °C) (Testo SE & Co. KGaA, Titisee-Neustadt, Germany) were embedded directly into the asphalt at fixed intervals. Temperature was logged at 1–5 min intervals during the daily heating–cooling cycle. Paired sensors were systematically positioned in shaded and sun-exposed micro-sites within the same road section to quantify the temperature differential and determine the thermal lag associated with persistent shadowing.

The integration of these two complementary measurement systems (high-resolution thermal imaging and direct contact thermometry) provided a robust multi-scale dataset for cross-validation. While the FLIR T540 imagery offered continuous spatial coverage, the Testo 110 sensors delivered precise temporal point data, enabling detailed quantification of the relationship between modelled solar exposure and observed pavement temperature. This combined evidence significantly reinforces the reliability and applicability of the proposed methodology.

2.3. Study Areas and Site Description

Four mountain road sections located in central and northern Spain were selected to validate the proposed methodology (Figure 3). These segments represent a range of geomorphological and infrastructural conditions that affect shadow persistence, including orientation, slope, elevation, and surrounding topography. All are located in areas where winter hazards (particularly frost and ice) frequently jeopardize road safety and necessitate intensive maintenance operations.

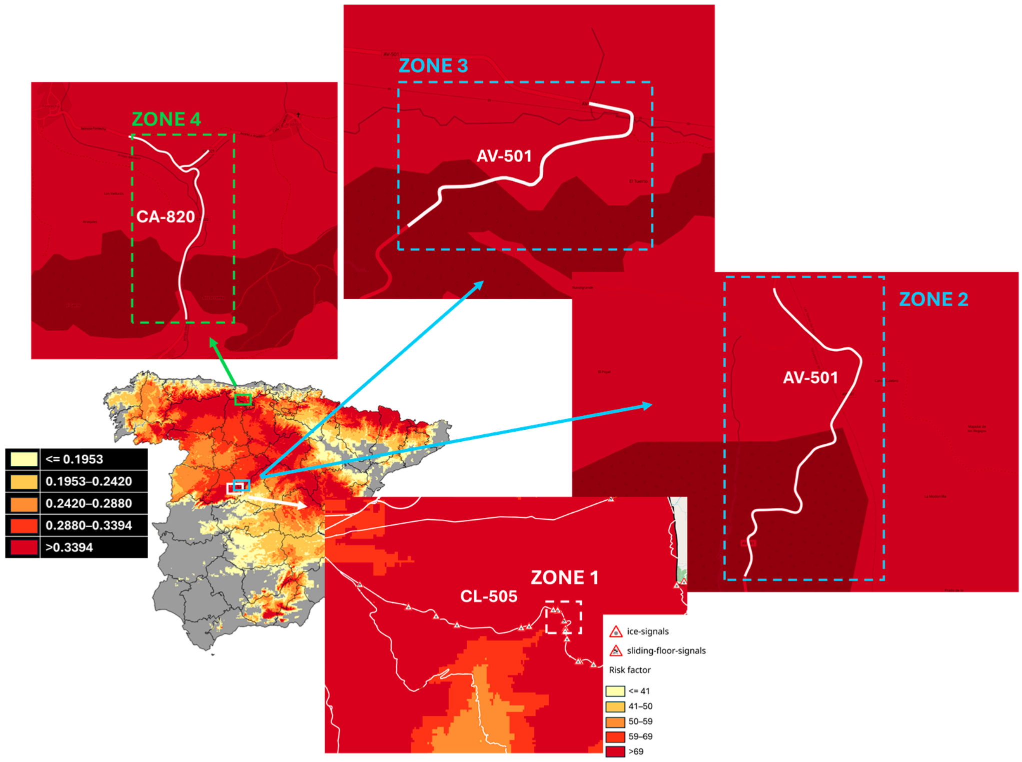

Figure 3. Location of the four study zones used for model validation. The background map represents the national Winter Risk Index (R_X), where red areas indicate higher exposure to frost and ice. Insets show the positions of the selected road segments: Zone 1 (CL-505, Ávila–Madrid corridor), Zones 2 and 3 (AV-501, located in the Sierra de Malagón within the broader Sierra de Guadarrama system), and Zone 4 (CA-820, Sierra de la Demanda).

2.3.1. Zone 1—CL-505 (Ávila (Ávila Province)—Community of Madrid)

The CL-505 connects the city of Ávila with the Community of Madrid, acting as a key communication axis between the northern Meseta Central and the metropolitan area of the Spanish capital. The road traverses a complex topographic gradient, descending from the Ávila highlands (above 1100 m a.s.l.) through successive terraces and valleys toward lower elevations. This altitudinal transition creates pronounced thermal contrasts and recurrent temperature inversions during the winter months.

Several segments of the CL-505 are north-facing or bordered by deep road cuts, limiting solar exposure and promoting persistent frost accumulation. Additionally, sections adjacent to forested embankments exhibit highly variable surface temperatures over short distances. These geomorphological and climatic characteristics make the CL-505 a particularly representative example of mountain roads affected by limited solar radiation.

2.3.2. Zone 2 and Zone 3—AV-501 (Aldeavieja—Navalperal de Pinares, Ávila Province)

Zones 2 and 3 correspond to two distinct segments of the AV-501, a regional road connecting the municipalities of Aldeavieja and Navalperal de Pinares. The route ascends through the Malagón mountain range, traversing the Puerto de la Lancha pass, a characteristic high-elevation corridor within this sector of the Sierra. This portion of the Sierra de Ávila features steep gradients, abrupt orientation changes, and significant variations in vegetation cover, all of which contribute to pronounced differences in solar exposure and surface temperature behavior.

Although both sections belong to the same stretch of the AV-501, their geomorphological settings differ substantially. Zone 2 is located on the southern slope of the Malagón range, with road orientations predominantly between the southeast and west, which allows for relatively favourable sun exposure under clear-sky conditions. However, the presence of dense forest cover and the steepness of the adjacent terrain significantly reduce this potential, creating extended shadow periods even during midday.

In contrast, Zone 3 lies on the northern slope, with orientations mainly between the north and east, a configuration that naturally limits direct solar radiation during winter months. Unlike Zone 2, this section is largely open and lacks vegetation cover, meaning that shading is controlled almost exclusively by the mountain's topography rather than canopy obstruction.

This clear dichotomy (south-facing but forested versus north-facing and open) provides an ideal framework for assessing how vegetation and slope aspect interact to modulate radiative inputs and microclimatic behaviour under otherwise comparable regional environmental conditions.

The Puerto de la Lancha, located above 1485 m a.s.l., frequently experiences persistent frost and snow accumulation, emphasizing the critical role of shadow persistence in winter road safety. The AV-501 alternates between open ridges exposed to direct sunlight and narrow valleys prone to extended shading, illustrating how micro-topographic variations modulate thermal response.

Zones 2 and 3 were therefore selected to assess the combined influence of orientation, slope, and vegetation on shadow duration and its spatial distribution. Compared with the CL-505, the AV-501 presents a more sinuous geometry and heterogeneous land cover, providing a robust test for evaluating the model's ability to capture local-scale differences in shadow persistence and thermal heterogeneity within mountainous road environments.

2.3.3. Zone 4—CA-820 (Reinosa–Fontecha, Cantabria Province)

The CA-820 is a regional mountain road located in Cantabria, connecting the towns of Reinosa and Fontecha. This stretch lies within a narrow valley system enclosed by steep mountain slopes that rise several hundred meters on both sides of the road. The alignment follows the natural topography of the valley floor, resulting in limited solar exposure for much of the day, particularly during winter months when the solar altitude is minimal.

Due to this enclosed configuration, the CA-820 represents one of the most critical scenarios for shadow persistence. The adjacent ridges cast long, continuous shadows, producing sections of pavement that remain under low or zero direct irradiance for extended periods, especially during morning and afternoon hours. In addition, temperature inversions are frequent, with cold air accumulating in the valley bottom, further reinforcing frost formation and ice stability.

The surrounding landscape alternates between pasture areas and patches of mixed forest, which contribute to differential heating and enhance microclimatic variability. These characteristics make the CA-820 an ideal site for testing the response of the shadow-detection model under conditions of extreme topographic confinement and minimal solar input. The following Table 1 provides an overview of the evaluated study areas.

https://doi.org/10.3390/rs18030476

Table 1. Main characteristics of the evaluated study areas.

	Zone 1	Zone 2	Zone 3	Zone 4
Length	850 m	2160 m	1340 m	1250 m
Altitude Range	Max: 1391 m Min: 1364 m	Max: 1429 m Min: 1337 m	Max: 1426 m Min: 1373 m	Max: 1008 m Min: 930 m
Aspect	NE, SE	SE-SW	NE	S
Vegetation	Dense, evergreen crown	Wide canopy, with leaf	Non-existent or almost non-existent	Scarce in the vicinity
Flight date and time	5 Nov 11:14 a 11:29	4 Nov 8:54 a 9:18	4 Nov 9:44 a 10:25	10 Nov 9:14 a 10:05

3. Results

3.1. Spatiotemporal Simulation of Solar Exposure Across the Four Mountain Roads

To characterize the influence of topography on winter solar availability, a continuous hourly simulation of solar incidence was performed for each of the four selected road segments (Zones 1–4). At every time step, the model evaluated the orientation, slope, and superelevation of the pavement, together with surrounding terrain geometry derived from the DTM02 (2 m DTM provided by the National Geographic Institute (IGN)) [34], to determine whether each cell received direct sunlight or was obstructed by terrain or vegetation.

The hourly outputs were subsequently aggregated to compute the total number of effective sunlight hours for a representative winter day. The resulting maps (Figure 4) reveal substantial differences in solar exposure between the analyzed roads, driven primarily by aspect variations, valley confinement, and slope asymmetry.

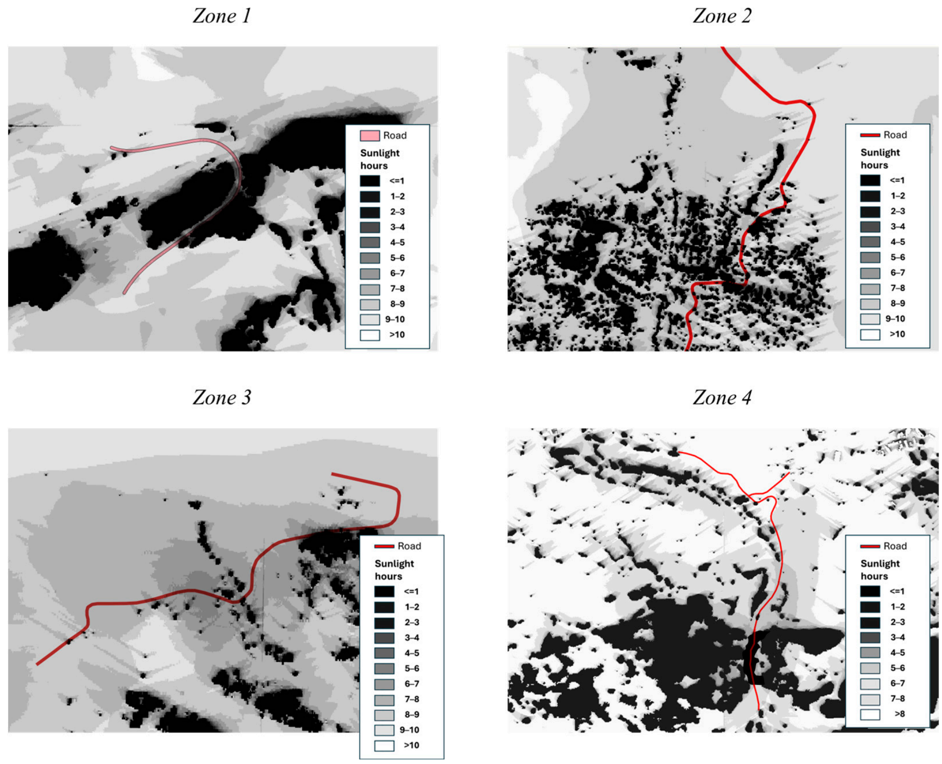

Figure 4. Winter cumulative sunlight hours along the four analysed mountain road segments. Light tones indicate longer solar exposure, while dark tones mark persistent shading caused by topography and vegetation. Top-left: Zone 1 (CL-505). Top-right: Zone 2 (AV-501 forested sector). Bottom-left: Zone 3 (AV-501 open sector). Bottom-right: Zone 4 (CA-820, Reinosa–Fontecha).

In the mentioned Figure 4, lighter tones denote segments with prolonged irradiance, while darker tones identify areas that remain in persistent shadow. These low-irradiance sectors correspond to locations where the pavement receives insufficient energy input to warm effectively during daytime, thereby increasing the probability of frost survival into late morning or even early afternoon.

Zone 1—CL-505 (Ávila–Madrid corridor)

The CL-505 displays alternating illuminated plateaus and deeply shadowed cuts. North-facing bends and steep embankments create continuous winter shading, particularly in the upper section approaching the Ávila plateau. These conditions align with field observations identifying this stretch as a recurrent site of frost persistence.

Zone 2—AV-501 (Forested south-oriented sector)

This segment, surrounded by dense woodland, shows an extensive distribution of shadows even during midday. Terrain shading is compounded by canopy obstruction, significantly limiting effective irradiance. As a result, several subsections accumulate less than two hours of daily sun exposure.

Zone 3—AV-501 (Open north-oriented sector)

Although located along the same road corridor as Zone 2, the microclimatic behavior of Zone 3 differs profoundly due to its topographic configuration. This section occupies a high-elevation slope oriented predominantly toward the northeast, a setting that inherently restricts winter solar incidence. Because the sun remains low along the southern horizon during the cold season, the pavement surface receives only brief and highly oblique radiation, resulting in near-permanent shading throughout the day.

Unlike Zone 2, where a south-facing aspect would typically allow substantial irradiance but is heavily mitigated by dense forest cover, Zone 3 has no vegetation capable of contributing additional shading. Nevertheless, its unfavorable aspect, elevation, and the shielding effect of the surrounding terrain combine to yield some of the lowest effective solar exposure values across the entire study area.

Zone 4—CA-820 (Reinosa–Fontecha, Cantabria)

This road shows the most extreme shading conditions. Enclosed between two steep mountain walls, large portions of the CA-820 remain in shadow throughout the day during winter. Some micro-valleys receive less than one hour of direct sunlight, confirming this area as an exceptionally cold corridor.

3.2. Solar Incidence and Shading Integration

To refine the assessment of winter solar availability, a second phase of analysis was conducted to integrate the effects of road geometry with the shadowing produced by surrounding terrain and vegetation. Unlike the cumulative sunlight hours shown in Figure 4, this stage focuses on the normalized solar incidence factor, which quantifies the proportion of potential irradiance a road segment actually receives once shading effects are applied.

The first step in the process involved calculating the theoretical irradiance expected from each segment solely on the basis of geometric parameters, namely slope, aspect, and superelevation. Under this configuration, roads facing south or southwest showed comparatively high incidence values, as their orientation allows for more direct interaction with the low winter sun.

However, when terrain- and vegetation-induced shading was incorporated into the model, the resulting irradiance distribution revealed substantial spatial variability that was not apparent from sunlight-hour maps alone. Even in road segments that receive a similar number of daylight hours, the effective solar input can differ markedly due to the combined influence of slope aspect, surrounding relief, and canopy obstruction. In several areas (particularly deeply incised valleys, densely forested corridors, and north-facing embankments), the persistent shading generated by adjacent terrain or vegetation significantly reduces the proportion of usable irradiance reaching the pavement. This demonstrates that equal exposure in terms of daylight duration does not necessarily translate into equal radiative conditions, as the geometric interaction among the solar path, slope orientation, and topographic obstacles plays a decisive role in modulating the real amount of energy available for surface heating.

- The largest discrepancies between theoretical irradiance and shadow-adjusted irradiance were observed in: Zone 1 (CL-505), where road cuts and north-facing curves significantly lower solar incidence;
- Zone 2 (AV-501, forested sector), where dense vegetation creates long periods of shade;
- Zone 3 (AV-501, open sector), where orientation remains the limiting factor rather than canopy obstruction;
- Zone 4 (CA-820, Reinosa–Fontecha), where the road's layout between two steep ridges produces shade almost all day.

These results underscore the importance of microtopographic confinement in determining the persistence of shadow and, consequently, the duration of surface freezing. Even when meteorological conditions are similar, the geometric configuration of each road segment produces markedly different irradiance regimes.

Following the hourly simulations, the shading and solar incidence maps were combined to generate an effective solar irradiance index normalized between 0 and 1 (Figure 5). This index integrates both the geometric incidence angle (θ) and atmospheric attenuation (as described in Section 2.3.1), providing a synthetic measure of the real energy input received by the pavement surface.

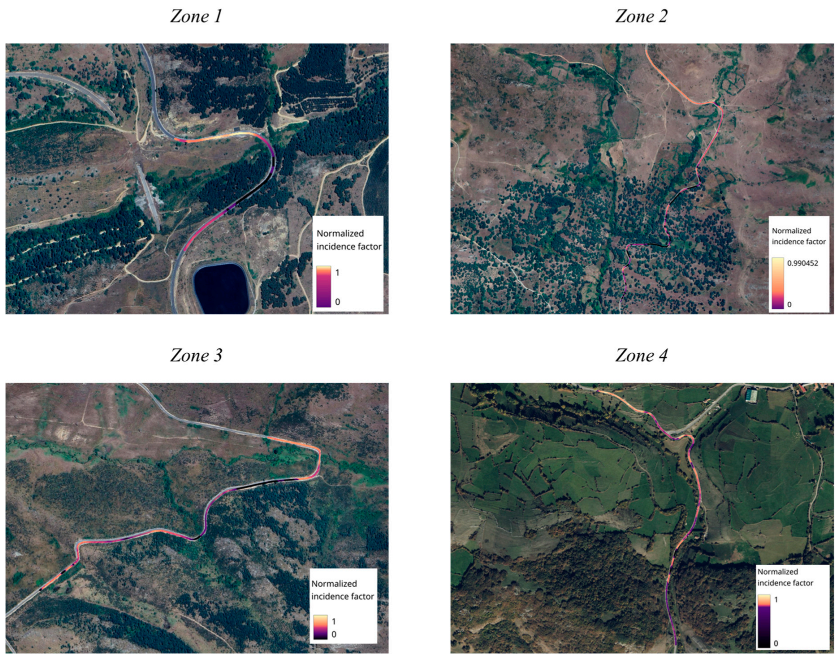

Figure 5. Combined solar incidence factor and shading maps for the four study areas. The composite index (0–1) is a normalized measure of relative irradiance that highlights which segments receive comparatively greater or lesser solar exposure. The colors reflect relative trends, not absolute energy values, so even small real differences are visually distinguishable, allowing for easy identification of critical areas of low irradiance.

The spatial distribution of this index shows that the combination of high slope and unfavorable orientation can reduce irradiance by more than 60%, even under clear-sky conditions. This attenuation is especially pronounced in concave terrain forms and densely forested sectors. In contrast, convex or open south-facing slopes maintain higher irradiance levels and therefore lower susceptibility to persistent frost.

3.3. UAV-Based Thermal Data Acquisition

Thermal surveys were conducted over the four study zones to obtain high-resolution radiometric data suitable for validating the modelled shadow and irradiance patterns (Figure 6). All flights were performed during October and November 2025, a period selected to ensure the presence of early-winter thermal conditions while maintaining operational safety.

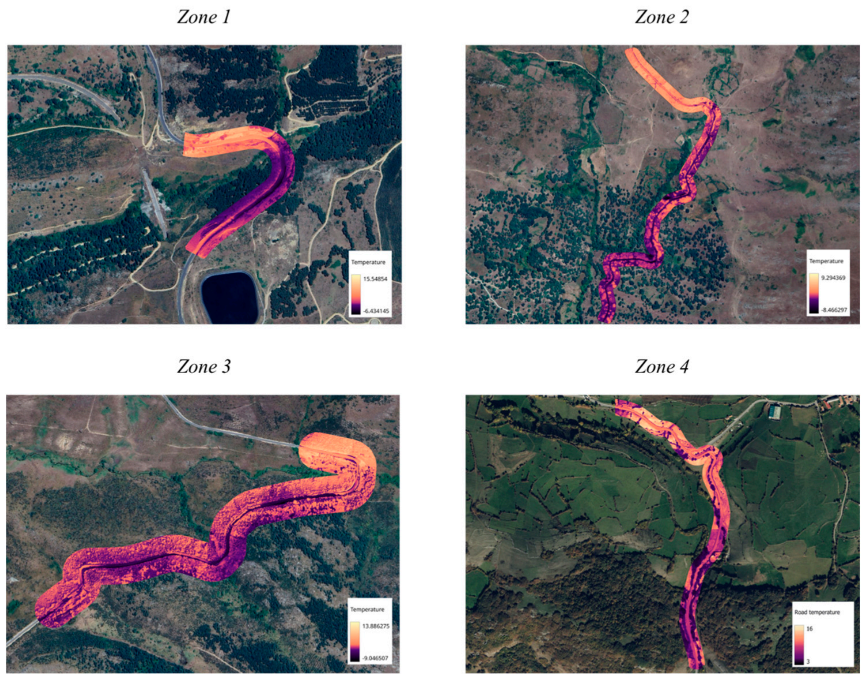

Figure 6. Thermal orthomosaics generated from UAV surveys conducted in October–November 2025 under low-wind conditions. All missions were flown at 100 m AGL with terrain-following based on a 1 m DTM, using a DJI Matrice 350 RTK and Zenmuse H20T thermal sensor. The final orthomosaics achieved a GSD of 10 cm.

To minimize geometric instability and thermal noise, flight operations were restricted to days without significant wind, and missions were run in the early hours of the day after sunrise, when pavement temperature gradients are more uniform and direct solar heating is still minimal.

A DJI Matrice 350 RTK equipped with a Zenmuse H20T multisensor payload (radiometric infrared, accuracy ±2 °C/±2%) was used for all acquisitions. Flights were performed at a constant altitude of 100 m above ground level, using a terrain-following mode based on a preloaded 1 m DTM (IGN). This ensured consistent ground sampling distance and correct imaging geometry across steep, mountainous segments.

Mission planning employed 80% forward overlap and 70% side overlap, guaranteeing sufficient redundancy for photogrammetric reconstruction. After acquisition, all thermal frames were processed using a structure-from-motion workflow adapted for radiometric imagery, including: radiometric correction of thermal frames, tie point extraction and bundle adjustment with RTK metadata, dense matching of thermal pixels, and thermal orthomosaic generation.

The final orthophotos achieved a Ground Sampling Distance (GSD) of approximately 10 cm, providing spatial detail adequate for identifying micro-scale temperature variations along the road surface.

The resulting radiometric orthomosaics serve as the reference dataset for validating the GIS-based shadow persistence model and for confirming the location of cold-prone road segments.

Once the thermal orthophotos were generated from the UAV surveys, an on-site validation campaign was carried out to verify the accuracy and radiometric consistency of the aerial temperature data. This validation was essential to confirm that the spatial patterns detected in the orthomosaics corresponded to real thermal conditions on the pavement surface.

Ground truth measurements were collected immediately after the flights using two complementary instruments:

- A FLIR T540 handheld thermal camera, used to capture oblique thermal images of the road surface. These images provided qualitative confirmation of temperature gradients, shadow-induced cooling, and the thermal contrast between sunlit and shaded sections.
- A calibrated Testo 110 contact thermometer, equipped with a surface probe, used to obtain precise point temperature readings directly on the asphalt. Measurements were taken at multiple points along the UAV flight path, including both shaded and illuminated segments.

To minimize temporal deviation between aerial and terrestrial data, field measurements were conducted within 30–45 min after UAV acquisition, as illustrated in Figure 7. Although small deviations may occur under rapidly changing thermal conditions, especially near sunrise, reducing the time gap further was not feasible given the flight conditions and operational constraints. The comparison between the contact measurements, ground-based thermal images, and UAV-derived temperatures showed strong agreement in the relative distribution of thermal patterns, indicating that the temporal gap does not significantly affect the comparability of the results.

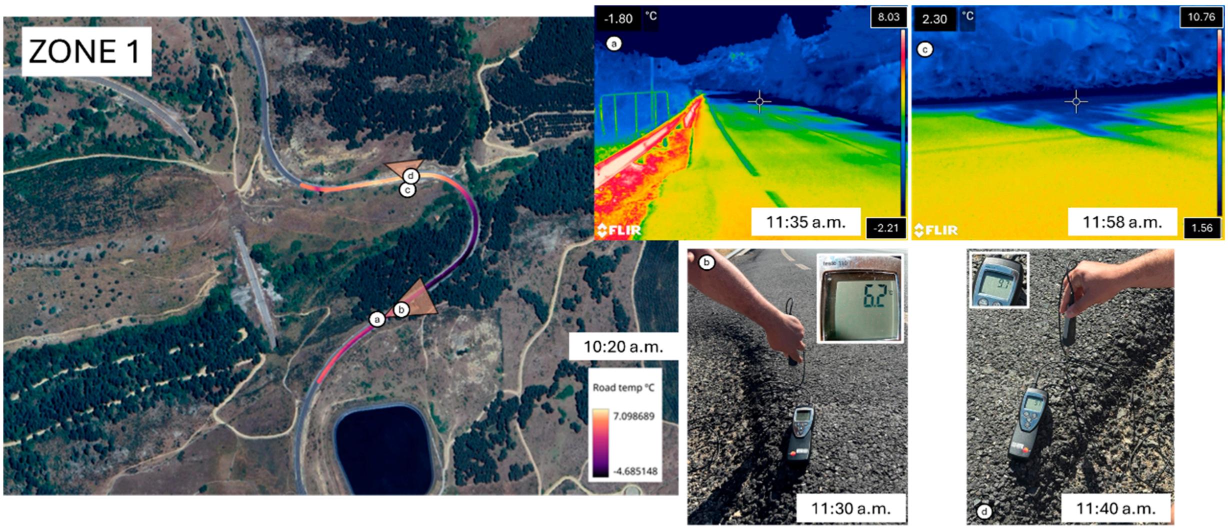

Figure 7. Ground validation of UAV-derived thermal orthophotos (Zone 1). (**a**) Location of measurement points along the surveyed road section. (**b**,**c**) Ground-based thermal images acquired with a FLIR T540 camera, showing temperature contrasts between shaded and illuminated pavement. (**d**) Contact measurements using a Testo 110 surface thermometer, obtained minutes after the UAV flight. The correspondence between UAV temperatures and field observations confirms the validity of the thermal orthomosaics.

Areas identified as cold zones in the orthophotos consistently corresponded to field-measured low temperatures, confirming the adequacy of the radiometric calibration and processing workflow.

This combined validation demonstrates that the thermal orthophotos accurately represent the spatial variability of pavement temperature and are suitable for evaluating shadow-induced cooling effects along mountainous road segments.

3.4. Comparison Between Modelled Irradiance and UAV Thermal Observations

To evaluate the reliability of the shadow–irradiance model, a comparative analysis was carried out between the normalized solar incidence index and the thermal orthomosaics generated from UAV surveys. Figure 8 provides a side-by-side visualization for each study area, where modeled irradiance patterns (left column) are directly contrasted with the corresponding road surface temperatures captured by the drone (right column).

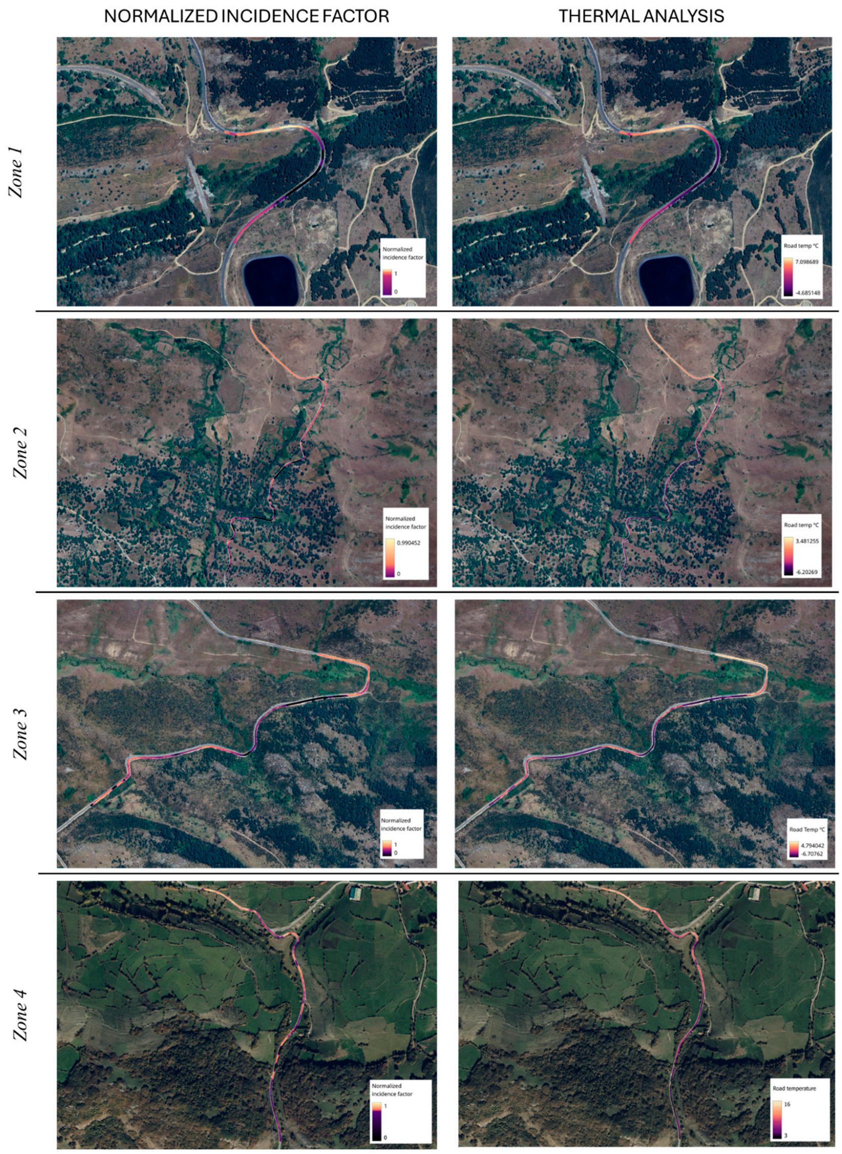

Figure 8. Comparison between the normalized solar incidence index (left column) and UAV-derived thermal orthomosaics (right column) for the four study zones. The spatial agreement between low-irradiance areas and colder pavement temperatures demonstrates strong consistency between modelled and observed patterns, validating the shadow-persistence detection methodology.

Despite describing fundamentally different physical quantities (irradiance potential vs. measured radiometric temperature) the spatial configuration of both datasets exhibits a consistent correspondence across the four zones. Locations identified by the model as low-irradiance sectors (purple tones) systematically align with the coldest areas in the thermal orthophotos.

This agreement is especially notable in:

- Zone 1 (CL-505), where shaded cut slopes and north-facing bends appear as continuous low-incidence corridors in the model and coincide with colder pavement strips in the UAV mosaics.
- Zone 2 (AV-501, forested segment), where the thermal data visibly reflects the cooling effect of dense canopy cover, matching the extensive shadow persistence predicted for the same sector.
- Zone 3 (AV-501, open segment), where thermal variations remain primarily governed by geometric orientation, again following the irradiance gradients simulated by the model.
- Zone 4 (CA-820, Reinosa–Fontecha), where the road is constrained between two steep ridges; both the irradiance map and the thermal orthophoto register a marked cooling pattern along these confined sections.

Across all four cases, the thermal observations corroborate the model's indication that topographic confinement, northward orientation, and forest canopy obstruction are the dominant drivers of surface cooling. The close spatial overlap between simulated low-irradiance zones and UAV-detected cold patches confirms that the method effectively captures the microclimatic behavior of each road segment.

This validation demonstrates the suitability of the proposed approach for identifying shadow-persistent road sections that are prone to frost retention. Moreover, the concordance between modeled irradiance potentials and thermal measurements supports the use of the shadow index as an operational proxy for winter hazard detection in road infrastructure.

4. Discussion

The combined evaluation of solar incidence, terrain-induced shading and UAV-based thermal observations demonstrate with high clarity that winter road behavior is governed by microtopographic and environmental conditions that operate at much finer scales than those captured by traditional climatic or meteorological datasets. While national or regional winter hazard models tend to focus on large-scale variables such as temperature, precipitation or elevation, the present study shows that the persistence of shadows (driven by slope configuration, valley geometry and vegetation cover) plays a decisive role in determining the capacity of pavement to warm during winter days. As a result, shadow persistence emerges as one of the most critical predictors of frost retention along mountainous roads, often outweighing the influence of purely climatic factors.

The spatial patterns identified across the four study areas reveal that microtopographic confinement exerts the strongest influence on winter solar availability. In deeply incised valleys, canyon-like sectors or narrow corridors bracketed by steep lateral slopes, sunlight is obstructed for most of the day regardless of the nominal orientation of the road surface. This phenomenon is clearly visible in Zones 1 and 4, where long-lasting shading persists even under completely clear skies. These environments create thermal bottlenecks where the pavement remains cold for extended periods, thereby extending the lifetime of frost patches and increasing the likelihood of ice formation during early morning or evening hours. Such behavior cannot be anticipated using meteorological records alone, underscoring the need for high-resolution topographic modelling.

The contrast between Zones 2 and 3 highlights the different mechanisms through which shading affects winter solar availability. Zone 2, located on the south-facing slope of the Malagón range, receives potentially abundant sunlight, but dense forest canopy and the surrounding relief reduce effective solar access during much of the day. In this case, vegetation plays a dominant role in prolonging shadow duration and moderating pavement warming.

In contrast, Zone 3 occupies a higher-elevation, north-facing slope where the terrain itself produces near-permanent shading. Here, the absence of forest cover does not translate into greater irradiance: the combination of unfavorable aspect, increased altitude, and the screening effect of the surrounding mountain geometry results in persistent low solar exposure, independent of land cover. This setting is known for maintaining frost and snow for extended periods, consistent with its orientation and cold microclimatic conditions.

The observed strong correspondence between modelled irradiance patterns and UAV-derived thermal orthomosaics, evaluated visually through spatial overlap, provides confidence in the validity of the simulation approach. The development of detailed numerical agreement metrics could be explored in future studies, as it requires a labor-intensive process of spatial and thermal data integration. Even though irradiance represents a theoretical potential for energy input and thermal data reflect instantaneous surface temperatures, both datasets exhibit highly consistent spatial patterns of cold-prone segments. Shaded curves, forested corridors, and narrow mountain passes appear identically as low-irradiance zones in the model and as cold patches in the thermal imagery. This convergence confirms that the irradiance model effectively captures the microclimatic behavior of pavement surfaces and can reliably predict areas with increased risk of frost persistence.

These findings have immediate and highly relevant implications for winter road management. Identifying the exact locations where shadows persist and where pavement temperatures remain low enables road authorities to prioritize maintenance efforts, allocate de-icing materials more efficiently, and plan targeted interventions during the hours of highest risk. This approach allows winter services to optimize their resources, reducing unnecessary salt spreading while focusing treatments on the stretches most likely to retain ice. Beyond operational efficiency, this contributes to increased road safety by enabling more accurate forecasting of hazardous conditions and earlier deployment of preventive actions such as the installation of warning signs or variable message panels.

In the current Spanish road management practice, warning signs for ice hazard ("Peligro por hielo") are typically installed only after maintenance crews have repeatedly observed frost formation on a given segment or once several accidents attributable to ice have already occurred. This reactive approach means that signage often appears only after hazardous conditions have already been demonstrated in the field. The methodology presented in this study offers a major improvement by enabling the proactive and assisted identification of shadow-dominated, cold-persistent road sections. By mapping these zones before incidents occur, road authorities can assign ice-warning signs strategically and early, reducing dependence on anecdotal observations and improving the overall prevention capacity of the road network.

The results of this research also hold significant strategic value for the national GEO-ROAD project [35], which focuses on developing geothermal-assisted heating systems for road infrastructure. The shadow and irradiance analysis presented here serves as a critical first step for the selection of candidate locations where pavement heating systems would be most beneficial. By identifying persistent cold zones with the highest exposure to shading and microclimatic cooling, the methodology makes it possible to pinpoint the road segments that would gain the greatest operational advantage from geothermal heating. This spatial preselection is essential because it allows engineers to restrict detailed geological, thermal and geotechnical investigations to only the most critical areas, thereby reducing project costs and improving the efficiency of system design.

Furthermore, understanding the degree of shading and the local energy deficit at each segment provides insight into the expected heating demand of future geothermal installations. Segments with extreme shadow persistence, such as those in Zones 1 and 4, will require higher heating loads and more robust thermal designs, whereas partially illuminated sectors like Zone 3 may allow for more moderate configurations. This makes irradiance modelling an indispensable tool for tailoring the technical characteristics of geothermal heating systems, including pipe layout, circulation rates, heat pump sizing and the expected seasonal performance of the installations. Additionally, combining shadow maps with geological information (such as bedrock depth, soil thermal conductivity and groundwater availability) will enable the GEO-ROAD project to evaluate the feasibility and long-term performance of each potential installation.

In a broader context, the methodology developed in this study contributes to the emerging field of climate-resilient road infrastructure. As winter conditions in many regions of Europe become increasingly variable due to climate change, the ability to quantify microclimatic drivers such as shadow persistence becomes essential for anticipating future risk patterns. Irradiance modelling can be combined with climate projections to estimate how changes in solar trajectory, cloud cover or snowmelt dynamics might alter frost persistence in the coming decades. This opens the door to long-term planning strategies in which road design, maintenance scheduling and heating technologies can be adapted to evolving environmental conditions.

It is convenient to clarify that different DTMs with different resolutions are used in this research. DTM25 is employed for the quantification of the winter risk. DTM02 is used for the calculation of the irradiance factor, providing sufficient spatial detail to resolve geometric and morphometric variations along the road. Finally, the 1 m DTM is preloaded in the drone to accurately determine its position during data acquisition.

Despite its strengths, the approach presented here is subject to certain limitations. Modelling assumes clear-sky conditions and does not directly account for atmospheric variability, such as cloudiness or wind-driven convective cooling, which may lead to overestimation of surface irradiance under certain conditions. Vegetation is treated as a static object, although seasonal leaf cover variations (particularly in deciduous forests) could influence shading patterns and local irradiance. UAV thermal surveys, while highly detailed, capture only morning conditions; this limited temporal sampling may reduce accuracy in capturing short-term thermal variations. Potential mitigations include performing repeated UAV flights under different times and seasonal conditions, incorporating dynamic vegetation models, and refining irradiance calculations with high-frequency solar position updates.

In summary, the integration of high-resolution solar radiation modelling, shadow persistence analysis and UAV-based thermal validation provides a powerful framework for understanding winter road hazards at the micro-segment scale. The research reveals how terrain geometry, slope orientation and vegetation interact to generate cold-persistent zones highly prone to frost formation. The demonstrated agreement between the models and thermal observations validates the methodology and confirms its suitability for both operational winter maintenance and long-term strategic planning. Importantly, the approach offers direct applications for public administration and critical added value for the GEO-ROAD project, where the identification of shadow-dominated road segments constitutes the foundation for designing geothermal road-heating systems. Through the precise detection of cold-prone areas, this methodology supports more efficient resource allocation, improves road safety, and advances the development of sustainable, low-carbon heating technologies for transportation infrastructure.

5. Conclusions

This study demonstrates that winter road hazard assessment cannot rely solely on large-scale climatic indicators but must incorporate high-resolution analyses of shadow persistence, terrain geometry and localized irradiance deficits. By integrating hourly solar incidence modelling with terrain-induced shading and validating the results through detailed UAV-based thermal orthophotos and ground measurements, the research provides a robust methodological framework capable of identifying microclimatic cold-persistent road segments with high spatial precision.

The four mountainous road sections analyzed exhibit markedly different irradiance regimes despite sharing similar regional climatic conditions. This variability is driven primarily by local topographic factors (such as valley confinement, slope asymmetry, embankments and cut slopes) as well as vegetation cover. The strong spatial correspondence between modelled low-irradiance zones and UAV-detected cold patches confirms that shadow persistence is one of the dominant controls on pavement temperature during winter, and thus a key predictor of frost survival and ice formation. The validation process demonstrates that the combined model reliably captures the microclimatic behavior of each segment, making it a dependable tool for operational decision-making.

From an applied perspective, the methodology provides actionable information for road authorities responsible for winter maintenance. The capacity to map, with geospatial accuracy, the segments most prone to shadow-induced cooling enables more efficient allocation of de-icing materials, targeted deployment of salt spreaders and snowploughs, and proactive risk mitigation in areas where frost is most likely to persist. Unlike general climatic datasets, the proposed approach identifies hazards at a scale that matches real maintenance operations, offering immediate operational benefits for public administrations and roadway managers.

Beyond winter service optimization, the results have further strategic impact within the framework of the current GEO-ROAD project. The detection of shadow-dominated corridors with recurrent cold persistence serves as a fundamental input for selecting suitable locations for geothermal-assisted road heating systems. By isolating the stretches with the highest thermal deficit, the model allows for precise planning of where heating infrastructures would be most effective. These priority zones then become candidates for deeper geological and geotechnical evaluation, ensuring that subsequent analyses and pilot installations focus on segments with the highest operational need and the most favorable subsurface characteristics. The irradiance maps also provide insight into the expected heating demand of each segment, supporting the design and optimization of geothermal configurations, including pipe arrangement, heat pump sizing and expected thermal performance.

Overall, the research highlights that integrating topographic modelling, solar analysis and UAV thermography can significantly advance our understanding of winter road dynamics. This multi-scale approach yields a level of diagnostic precision not attainable through conventional meteorological monitoring and opens new pathways for designing infrastructure-level climate resilience strategies. As climatic variability continues to alter winter patterns across Europe, methodologies capable of capturing microclimatic drivers (such as shadow persistence) will be essential for ensuring safe and sustainable transportation networks.

Future research should aim to incorporate seasonal changes in vegetation, cloud cover variability, and continuous multi-temporal UAV surveys to further refine the model. Nevertheless, the results presented here provide compelling evidence that shadow-based hazard mapping is a valuable and operationally mature tool for winter road management, maintenance planning and the development of next-generation geothermal heating technologies for cold-prone mountain infrastructure.

Author Contributions: Conceptualization, M.Á.M.-G. and C.S.B.; methodology, M.Á.M.-G., C.S.B. and D.H.H.; software, M.Á.M.-G. and D.H.H.; validation, M.Á.M.-G., C.S.B. and D.H.H.; formal analysis, M.Á.M.-G. and D.H.H.; investigation, M.Á.M.-G., C.S.B. and D.H.H.; resources, M.Á.M.-G.; data curation, D.H.H. and S.A.C.V.; writing—original draft preparation, M.Á.M.-G., C.S.B. and D.H.H.; writing—review and editing, M.Á.M.-G., C.S.B. and I.M.N.; visualization, D.H.H. and S.A.C.V.; supervision, M.Á.M.-G. and C.S.B.; project administration, M.Á.M.-G.; funding acquisition, M.Á.M.-G. and C.S.B. All authors have read and agreed to the published version of the manuscript.

Funding: This research was supported by the GEO-ROAD project (PID2022-142097OA-I00), funded by the Ministerio de Ciencia e Innovación and by the European Union 'NextGenerationEU'/PRTR. Miguel Ángel Maté-González and Cristina Sáez Blázquez acknowledge the grants RYC2021-034813-I and RYC2021-034720-I, respectively, funded by the Ministerio de Ciencia e Innovación and by the European Union 'NextGenerationEU'/PRTR.

Data Availability Statement: The original contributions presented in the study are included in the article, and further inquiries can be directed to the corresponding author.

Acknowledgments: The authors gratefully acknowledge the Escuela Politécnica Superior de Ávila for facilitating access to its equipment and facilities for the completion of this work.

Conflicts of Interest: The authors declare no conflicts of interest.

References

1. Fu, L.; Usman, T.; Miranda-Moreno, L.F.; Perchanok, M.S.; McClintock, H. How much is the safety and mobility benefit of winter road maintenance? In Proceedings of the 2012 Conference of the Transportation Association of Canada, Fredericton, NB, Canada, 14–17 October 2012; pp. 14–17.
2. Fu, L.; Usman, T. Safety effects of winter weather and road maintenance operations. In *Sustainable Winter Road Operations*; Elsevier: Amsterdam, The Netherlands, 2018; pp. 101–130.
3. Hatamzad, M.; Polanco Pinerez, G.; Casselgren, J. Addressing uncertainty by designing an intelligent fuzzy system to help decision support systems for winter road maintenance. *Safety* **2022**, *8*, 14. [CrossRef]
4. Darghiasi, P.; Zamanian, M.; Shahandashti, M. Enhancing winter maintenance decision making through deep learning-based road surface temperature estimation. In *Construction Research Congress 2024*; ASCE: Reston, VA, USA, 2024; pp. 701–711.
5. Ruiz-Arias, J.A.; Tovar-Pescador, J.; Pozo-Vázquez, D.; Alsamamra, H. A comparative analysis of DEM-based models to estimate the solar radiation in mountainous terrain. *Int. J. Geogr. Inf. Sci.* **2009**, *23*, 1049–1076. [CrossRef]
6. Allard, R.F. Climate change adaptation: Infrastructure and extreme weather. In *Industry, Innovation and Infrastructure*; Springer: Cham, Switzerland, 2021; pp. 105–116.
7. Martín, B.; Ortega, E.; Cuevas-Wizner, R.; Ledda, A.; De Montis, A. Assessing road network resilience: An accessibility comparative analysis. *Transp. Res. Part D* **2021**, *95*, 102851. [CrossRef]
8. Xu, L.; Li, Y.; Wang, X.; Liu, L.; Ma, M.; Yang, J. A machine learning approach to estimating solar radiation shading rates in mountainous areas. *Sustainability* **2024**, *16*, 931. [CrossRef]
9. Neumann, J.E.; Chinowsky, P.; Helman, J.; Black, M.; Fant, C.; Strzepek, K.; Martinich, J. Climate effects on US infrastructure: The economics of adaptation for rail, roads, and coastal development. *Clim. Change* **2021**, *167*, 44. [CrossRef] [PubMed]
10. Navarro-Moreno, J.; Calvo-Poyo, F.; De Oña, J. Influence of road investment and maintenance expenses on injured traffic crashes in European roads. *Int. J. Sustain. Transp.* **2023**, *17*, 649–659. [CrossRef]
11. Fay, L.; Shi, X. Environmental impacts of chemicals for snow and ice control: State of the knowledge. *Water Air Soil Pollut.* **2012**, *223*, 2751–2770. [CrossRef]
12. de Abreu, V.H.S.; Santos, A.S.; Monteiro, T.G.M. Climate change impacts on the road transport infrastructure: A systematic review on adaptation measures. *Sustainability* **2022**, *14*, 8864. [CrossRef]
13. Sadeghi, P.; Goli, A. Investigating the impact of pavement condition and weather characteristics on road accidents. *Int. J. Crashworthiness* **2024**, *29*, 973–989. [CrossRef]

14. Yang, M.; Zhao, Y.; Li, C.; Yang, J. A review of spatiotemporal variations in temperature and precipitation: Trend analysis, driving mechanisms, and methodological evaluation. *Adv. Resour. Res.* **2024**, *4*, 836–859.
15. Hong, S.B.; Lee, B.W.; Kim, C.H.; Yun, H.S. System dynamics modeling for estimating the locations of road icing using GIS. *Appl. Sci.* **2021**, *11*, 8537. [CrossRef]
16. Jin, M.; McBroom, D.G. Investigating road ice formation mechanisms using road weather information system (RWIS) observations. *Climate* **2024**, *12*, 63. [CrossRef]
17. Scheer, J.; Tomaškovičová, S.; Ingeman-Nielsen, T. Thaw settlement susceptibility mapping for roads on permafrost: Towards climate-resilient and cost-efficient infrastructure in the Arctic. *Cold Reg. Sci. Technol.* **2024**, *220*, 104136. [CrossRef]
18. Yetemen, O.; Istanbulluoglu, E.; Flores-Cervantes, J.H.; Vivoni, E.R.; Bras, R.L. Ecohydrologic role of solar radiation on landscape evolution. *Water Resour. Res.* **2015**, *51*, 1127–1157. [CrossRef]
19. Kwon, H.G.; Yang, H.; Yi, C. Study on radiative flux of road resolution during winter based on local weather and topography. *Remote Sens.* **2022**, *14*, 6379. [CrossRef]
20. Verfaillie, M.; Cho, E.; Dwyre, L.; Khan, I.; Wagner, C.; Jacobs, J.M.; Hunsaker, A. UAS remote sensing applications to abrupt cold region hazards. *Front. Remote Sens.* **2023**, *4*, 1095275. [CrossRef]
21. Zhang, S.; Li, X.; She, J.; Peng, X. Assimilating remote sensing data into GIS-based all-sky solar radiation modeling for mountain terrain. *Remote Sens. Environ.* **2019**, *231*, 111239. [CrossRef]
22. Malbeteau, Y.; Johansen, K.; Aragon, B.; Al-Mashhawari, S.K.; McCabe, M.F. Overcoming the challenges of thermal infrared orthomosaics using a swath-based approach to correct for dynamic temperature and wind effects. *Remote Sens.* **2021**, *13*, 3255. [CrossRef]
23. Hoffrén, R.; García, M.B. Thermal unmanned aerial vehicles for the identification of microclimatic refugia in topographically complex areas. *Remote Sens. Environ.* **2023**, *286*, 113427. [CrossRef]
24. Pech, K.; Stelling, N.; Karrasch, P.; Maas, H.G. Generation of multitemporal thermal orthophotos from UAV data. *Int. Arch. Photogramm. Remote Sens. Spatial Inf. Sci.* **2013**, *40*, 305–310. [CrossRef]
25. Pfetsch, S.; Ragheb, T.; Laska, J.; Nejati, H.; Gilbert, A.; Strauss, M.; Massoud, Y. On the feasibility of hardware implementation of sub-Nyquist random-sampling-based analog-to-information conversion. In Proceedings of the IEEE International Symposium on Circuits and Systems (ISCAS), Seattle, WA, USA, 18–21 May 2008; pp. 1480–1483.
26. Kasten, F.; Young, A.T. Revised optical air mass tables and approximation formula. *Appl. Opt.* **1989**, *28*, 4735–4738. [CrossRef] [PubMed]
27. Moediartianto, A.; Montazeri, H.; Blocken, B. On the use of UAV-thermal imaging for CFD validation of urban thermal microclimate. *Sustain. Cities Soc.* **2025**, *106*, 106968. [CrossRef]
28. Lopez-Cabeza, V.P.; Videras-Rodriguez, M.; Gomez-Melgar, S.; Andujar-Marquez, J.M. Methodology for the use of aerial thermography as a validation method for outdoor thermal comfort simulations. *Energy Convers. Manag. X* **2025**, *28*, 101257. [CrossRef]
29. Jenčo, M. Determination of the solar angle of incidence using an equivalent surface and the possibility of applying this approach in geosciences and engineering. *ISPRS Int. J. Geo-Inf.* **2025**, *14*, 323. [CrossRef]
30. Blanc, P.; Espinar, B.; Geuder, N.; Gueymard, C.; Meyer, R.; Pitz-Paal, R.; Wilbert, S. Direct normal irradiance-related definitions and applications: The circumsolar issue. *Sol. Energy* **2014**, *110*, 561–577. [CrossRef]
31. Solla, M.; Maté-González, M.Á.; Sáez Blázquez, C.; Lagüela-López, S.; Nieto, I.M. Analysis of structural integrity through the combination of non-destructive testing techniques in heritage inspections: The study case of San Segundo's Hermitage (Ávila, Spain). *J. Build. Eng.* **2024**, *89*, 109295. [CrossRef]
32. Maté-González, M.Á.; Sáez Blázquez, C.; Camargo Vargas, S.A.; Peral Fernández, F.; Herranz Herranz, D.; González González, E.; González-Aguilera, D. Integrating advanced technologies for environmental valuation in legacy mining sites: The role of digital twins at Lavrion Technological and Cultural Park. *Sensors* **2025**, *25*, 5941. [CrossRef]
33. Gonzalez-Aguilera, D.; López-Fernández, L.; Rodriguez-Gonzalvez, P.; Hernandez-Lopez, D.; Guerrero, D.; Remondino, F.; Menna, F.; Nocerino, E.; Toschi, I.; Ballabeni, A. GRAPHOS—Open-source software for photogrammetric applications. *Photogramm. Rec.* **2018**, *33*, 11–29. [CrossRef]
34. Instituto Geográfico Nacional–Centro Nacional de Información Geográfica. *Modelo Digital del Terreno 2 m (MDT02)*; Gobierno de España: Madrid, Spain, 2025. Available online: https://centrodedescargas.cnig.es/ (accessed on 2 December 2025).
35. Vargas, S.A.C.; Sáez Blázquez, C.; Herranz, D.H.; Maté-González, M.Á. High-resolution mapping of shallow geothermal resources in Spain through multivariate spatial analysis. *Geothermics* **2026**, *134*, 103524. [CrossRef]